J Biomol NMR (2012) 54:389–400
DOI 10.1007/s10858-012-9682-x

ARTICLE

# A study on the influence of fast amide exchange on the accuracy of $^{15}$N relaxation rate constants

**Simon Jurt · Oliver Zerbe**

Received: 30 March 2012 / Accepted: 2 November 2012 / Published online: 10 November 2012


**Abstract** $^{15}$N relaxation rates of amide moieties provide insight both into global as well as local backbone dynamics of peptides and proteins. As the differences in the relaxation rates in general are small, their accurate determination is of prime importance. One potential source of error is fast amide exchange. It is well known that in its presence the effects of saturation transfer and H/D exchange may result in erroneous apparent relaxation rates $R_1$ and $R_2$. Here, the extent of these errors is rigorously examined. Theoretical considerations reveal that even when saturation effects are absent, H/D exchange will easily result in significant deviations from the true values. In particular overestimations of up to 10 % in $R_1$ and up to 5 % in $R_2$ are observed. An alternative scheme for fitting the relaxation data to the corresponding exponentials is presented that in the best cases not only delivers more accurate relaxation rates but also allows extracting estimates for the exchange rates. The theoretical computations were tested and verified for the case of ubiquitin.

**Keywords** $^{15}$N relaxation · Saturation transfer · H/D exchange · Ubiquitin

**Electronic supplementary material** The online version of this article (doi:10.1007/s10858-012-9682-x) contains supplementary material, which is available to authorized users.

S. Jurt · O. Zerbe (✉)
Institute of Organic Chemistry, University of Zurich, Winterthurerstrasse 190, 8057 Zurich, Switzerland
e-mail: oliver.zerbe@oci.uzh.ch

## Introduction

Relaxation parameters reveal information about dynamic properties at residue resolution (Abragam 1961; Cavanagh et al. 1996). In order to study backbone dynamics of peptides and proteins it has become routine to measure amide $^{15}$N longitudinal and transverse relaxation rates ($R_1$,$R_2$) as well as the $^{15}$N–{$^1$H} NOE (Dayie et al. 1996; Fischer et al. 1998; Korzhnev et al. 2001; Morin 2011), often at multiple field strengths. From such relaxation data local and overall backbone dynamics can be derived. For example an analysis following the model-free approach (Lipari and Szabo 1982) provides information about overall molecular rotational diffusion, rates as well as spatial restrictions of local NH motions, and contributions from chemical exchange.

Clearly, a realistic picture of backbone dynamics can only be obtained if relaxation parameter are measured in an accurate way (Jin et al. 1998; Fischer et al. 1998). Therefore numerous attempts have been made during the last two decades to improve experimental schemes for measuring relaxation parameters, e.g. by suppressing dipole/CSA cross correlation (Boyd et al. 1990; Kay et al. 1992; Palmer III et al. 1992; Myint et al. 2009) or cross relaxation (Dellwo and Wand 1991) effects, by using sensitivity-enhancement schemes for improved signal-to-noise (Palmer et al. 1991) and by minimizing heating effects (Yip and Zuiderweg 2005). In addition, the influence of pulse-offset effects (Ross et al. 1997; Korzhnev et al. 2000; Yip and Zuiderweg 2004; Myint et al. 2009) and chemical exchange (Carver and Richards 1972) during the CPMG sequence is well described. In order to minimize errors due to system or sample instabilities and to average out effects from sample heating (Orekhov et al. 1999) spectra are preferably recorded in an interleaved fashion.

Under optimal conditions $R_1$ and $R_2$ relaxation rates can be measured today within an error of a few percent.

Additional attention must be paid in the presence of fast amide proton exchange. The impact of water saturation transfer has been closely examined for the case of the $^{15}$N–{$^1$H} NOE experiment (Grzesiek and Bax 1993; Li and Montelione 1994; Idiyatullin et al. 2001), and its influence during $R_1$ and $R_2$ experiments has been mentioned but not quantified (Li and Montelione 1993; Farrow et al. 1995). In contrast, the effect of H/D exchange during the relaxation period in $R_1$ and $R_2$ experiments is investigated in much less detail (Chevelkov et al. 2008). Such effects are likely to be small for amide moieties in well-folded proteins, particularly when data are recorded at low pH. However, during a recent study of a protein devoid of much secondary structure conducted at a relatively elevated pH in our lab we discovered that H/D exchange might present an issue. This has stimulated us to initiate a detailed study of errors in $R_1$ and $R_2$ rates due to saturation transfer and H/D exchange. The exact magnitude of errors depends on many variables, such as the sampled time points as well as a lot of instrumental and experimental parameters. Therefore the error analysis is rather intended to provide an estimate on the magnitude of the errors that can be expected.

The effects by which $R_1$ and $R_2$ experiments are affected by amide proton/solvent exchange can be classified into three categories, that are: (i) saturation transfer during the inter-scan delay (ii) loss of detectable NH sites due to H/D exchange during the relaxation period and (iii) H/D fraction weighted averaging of protonated and deuterated amide $^{15}$N relaxation rates. In the following we describe these issues in more detail:

(i) If no care is taken to prevent perturbation of water magnetization in the course of $^1$H decoupling during the relaxation period, water magnetization becomes gradually saturated. During the inter-scan delay this saturation may then be transferred to amide protons directly through H/H exchange or indirectly via the NOE with an exchanging proton in proximity. As a consequence signal intensities are distorted and erroneous relaxation rates are obtained from least squares fits. (ii) Another error results from H/D exchange during the relaxation period. Briefly, amide $^1$H magnetization is initially transferred by the INEPT to $^{15}$N and following the relaxation period, back to $^1$H in the reverse-INEPT element. The fraction of protons replaced by deuterons during the sequence results in an additional decay of $^{15}$N magnetization adding to the apparent $^{15}$N relaxation such that the fitted relaxation rate is overestimated. The effect of H/D exchange has been noted by Chevelkov et al. (2008) for the case of $R_1$ experiments in solid-state NMR, and its potential for measuring H/D exchange rates has been recognized by del Amo et al. (2010) for solid-state NMR and by Chevelkov et al. (2010) for liquid-state NMR. (iii) Because the relaxation rates of protonated and deuterated $^{15}$N nuclei are different, the signal decay in the presence of H/D exchange will present a mixture of both relaxation rates. As the $^{15}$N relaxation rates of deuterated moieties are smaller the apparent relaxation rates are underestimated.

## Theory

Following an initial polarization transfer $^{15}$N magnetization in the $R_1$-experiment is rotated to the positive and negative $z$-axis in alternate scans and the difference is recorded so that the intensity $I$ of the crosspeaks is described in both experiments by a mono-exponential decay

$$I_{(\tau)} = I_0 e^{-R\tau} \quad (1)$$

The relaxation rates are extracted from least squares fits to the measured signal intensities obtained for many different τ's or at least for two τ's (at time zero and 1.3 times the expected relaxation time constants $T$) (Jones et al. 1996). In the following we will describe the effects of fast amide exchange on the accuracy of the derived relaxation rates.

### $^{15}$N-relaxation in the presence of H/D exchange (effects *ii* and *iii*)

Suppose an amide group undergoes exchange with protons and deuterons of the solvent characterized by the exchange rate constant $k$. At equilibrium a constant fraction $x$ of deuterated amide nitrogens, depending on the relative $D_2O$ content and the fractionation factor ϕ that accounts for different stabilities of the NH and ND bonds (LiWang and Bax 1996), is present.

$$x = \frac{\phi[\mathrm{D}]}{[\mathrm{H}] + \phi[\mathrm{D}]} \quad (2)$$

with [D] and [H] the mole fraction of $D_2O$ and $H_2O$ respectively. The change of $^{15}$N-magnetization with an attached proton ($M^{N(H)}$) or deuteron ($M^{N(D)}$) due to relaxation and H/D exchange during the relaxation period is described by the following coupled differential equations (for simplicity we neglect H/D exchange during the INEPT elements and shift evolution times which are of relatively short and constant duration in each experiment)

$$\frac{d}{dt}M^{N(H)} = -R^{N(H)}(M^{N(H)} - M_{eq}^{N(H)}) - kxM^{N(H)} + k(1-x)M^{N(D)} \quad (3a)$$

$$\frac{d}{dt}M^{N(D)} = -R^{N(D)}(M^{N(D)} - M_{eq}^{N(D)}) - k(1-x)M^{N(D)} + kxM^{N(H)} \quad (3b)$$

where $R^{N(H)}$ and $R^{N(D)}$ are the longitudinal or transverse relaxation rate constants, $k$ the exchange rate and $M_{eq}^{N(H)}$ and $M_{eq}^{N(D)}$ denote the equilibrium $^{15}$N $z$- or $xy$-magnetization of protonated and deuterated amide nitrogen nuclei, respectively. Taking into account that the initial nitrogen magnetization of the deuterated species makes an negligible contribution to the final signal, thus $M_{(t=0)}^{N(D)} \approx 0$, and solving equations 3a and 3b with $M_{(t=0)}^{N(H)} = M_0$ (for the $R_2$-experiment) or once with $M_{(t=0)}^{N(H)} = M_0$ and once with $M_{(t=0)}^{N(H)} = -M_0$ and subsequently taking the difference of the two solutions divided by two (for the $R_1$-experiment) one obtains in both cases

$$M_{(t)}^{N(H)} = M_0\left[\cosh\left(\frac{g}{2}t\right) - \frac{1}{g}(k(2x-1)+\Delta R)\sinh\left(\frac{g}{2}t\right)\right] \times e^{-\frac{R^{N(H)}+R^{N(D)}+k}{2}t} \quad (4)$$

with

$$g = \sqrt{\Delta R^2 + 2k(2x-1)\Delta R + k^2}$$

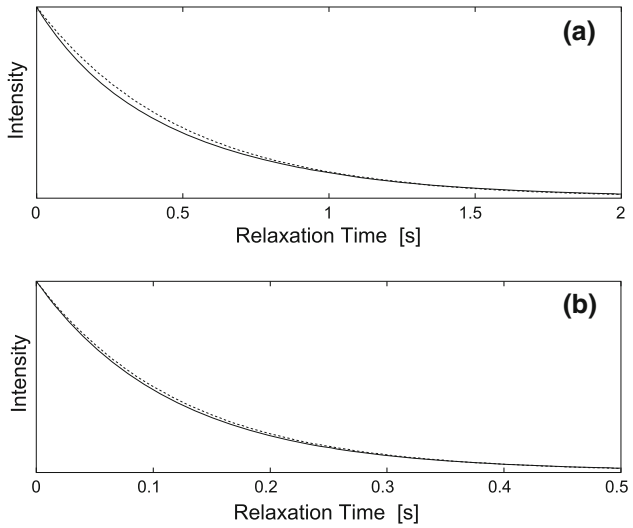


**Fig. 1** Longitudinal (**a**) and transverse (**b**) $^{15}$N relaxation curves in the presence of H/D exchange ($k = 5\ s^{-1}$) are shown by *solid lines*. The *curves* were calculated on the basis of Eq. 4 with **a** $R_1^{N(H)} = 2s^{-1}$, $R_1^{N(D)} = 1s^{-1}$ and **b** $R_2^{N(H)} = 8s^{-1}$, $R_2^{N(D)} = 3s^{-1}$ and $x = 0.1$ in both cases. For comparison the exponential decays in the absence of H/D exchange ($k = 0s^{-1}$) are depicted with *dashed lines*

and

$$\Delta R = R^{N(H)} - R^{N(D)}$$

Accordingly, relaxation in the presence of H/D exchange is no longer mono-exponential. It should be noted that evolution of magnetization during the relaxation period of the $R_2$ experiment is not straightforward to compute, and evolution due to shift and scalar coupling during the CPMG sequence must be considered. In particular scalar relaxation due to fast quadrupole relaxation of deuterium (Liwang and Bax 1997) and the isotope shift due to H/D exchange must be taken into account. Numerical integration of differential equations that consider such effects however demonstrate that when using short CPMG echo times $\tau_{cp}$ of about 0.5 ms Eq. 4 applies reasonably well (see Supplementary Material).

The deviation from mono-exponential decay is demonstrated for the particular case when $k = 5s^{-1}$ in Fig. 1. The maximum intensity difference between the analytical functions is 4 % in the case of $R_1$ and 2 % in the case of $R_2$ relative to the maximum signal. Similar calculations for exchange rates in the range of 1–10 $s^{-1}$ reveal that differences in the range of 1–6 % for $R_1$ and 0.4–3 % for $R_2$ can be expected.

## Water saturation transfer during the inter-scan delay (effect *i*, *ii* and *iii*)

Another systematic error is introduced if no special care is taken to prevent water saturation in the course of $^1$H decoupling during the relaxation period $\tau$. In that case water magnetization will be saturated as a function of $\tau$ and transferred by H/H exchange to the amide protons during the inter-scan delay. The extent of water saturation in general largely depends on the particular decoupling sequence, the probe in use and the sample conditions. In the following we will describe the water saturation by a factor $p$ that accounts for the relative extent by which thermal equilibrium water magnetization $M_{eq}^W$ is saturated through the decoupling to yield the steady-state magnetization $M_0^W$ at the start of the inter-scan delay, thus $M_0^W = p_{(\tau)}M_{eq}^W$ with $0 \leqq p_{(\tau)} \leqq 1$. The amide proton $z$-magnetization $M$ during the inter-scan delay accounting for saturation transfer is characterized by

$$\frac{d}{dt}M = -R_1^H(M - M_{eq}) - k\left(M - M^W\frac{M_{eq}}{M_{eq}^W}\right) \quad (5)$$

where $R_1^H$ is the longitudinal relaxation rate constant of the amide proton, $M_{eq}$ the equilibrium amide proton magnetization and $M^W$ the $z$-magnetization of water. $M^W$ during the inter-scan delay is given by

$$M_{(t)}^W = (M_0^W - M_{eq}^W)e^{-R_1^W t} + M_{eq}^W \quad (6)$$

with $R_1^W$ being the longitudinal relaxation rate constant of water. Substituting Eq. 6 into Eq. 5, with the initial

conditions $M_{(t=0)} = 0$ and $M_0^W = p_{(\tau)} M_{eq}^W$ the amide proton magnetization is expressed as

$$M_{(t)} = M_{eq}\left[1 - \frac{\left(R_1^H - R_1^W + p_{(\tau)}k\right)\mathrm{e}^{-\left(R_1^H+k\right)t}}{R_1^H - R_1^W + k} + \frac{k\left(p_{(\tau)} - 1\right)\mathrm{e}^{-R_1^W t}}{R_1^H - R_1^W + k}\right] \quad (7)$$

For a given inter-scan delay $d$, $M_{(d)}$ denotes the magnetization that is transferred to the amide nitrogen by the refocused INEPT element. When substituting $M_0$ of Eq. 4 by $M_{(d)}$ we obtain a rather involved expression which describes the signal intensity in dependence of the relaxation period τ. Figure 2 depicts such a $R_1$ relaxation curve for which saturation transfer is taken into account. The used parameters are the same as those of Fig. 1a, in addition we used typical values of our cryoprobe such as $R_1^H = 2\mathrm{s}^{-1}$, $R_1^W = 0.4\mathrm{s}^{-1}$, $d = 2$ s, $p_{(\tau)} = 0.75e^{-1.7\tau}$ (see Supplementary Material) and $M_{eq} = 1$. Note, the initial amplitude is attenuated due to the overall water saturation during the sequence even in the case where $\tau = 0$ ($p_{(0)} = 0.75$), the dashed curve is accordingly corrected for this. The maximum difference between the solid and dashed line is about 10 % relative to the maximum signal intensity. While in the case of the $R_1$ experiments $p(\tau)$ follows closely an exponential decay, in the $R_2$-experiment $p_{(\tau)}$ is not a simple exponential decay but a more complicated function that can be roughly approximated by the polynomial $0.7 + 0.24\tau - 2.7\tau^2$ (see Supplementary Material). Interestingly, the variation of the initial water magnetization is much smaller than in the case of the $R_1$ experiment.

The loss of amide $^{15}$N magnetization due to H/D exchange can be circumvented if the experiment is modified to start with equilibrium $^{15}$N magnetization at the expense of an up to 10-fold lower sensitivity. Because relaxation rates of deuterated nitrogens are smaller than in their protonated counterpart (see below) the effective relaxation of protonated amids is reduced in the presence of H/D exchange. A treatment similar to the one described above results in

$$M_{(t)}^{N(H)} = M_0(1-x)\left[\cosh\left(\frac{g}{2}t\right) - \frac{1}{g}(\Delta R - k)\sinh\left(\frac{g}{2}t\right)\right] \times \mathrm{e}^{-\frac{R^{N(H)}+R^{N(D)}+k}{2}t}$$

with $g$ and $\Delta R$ defined in Eq. 4.

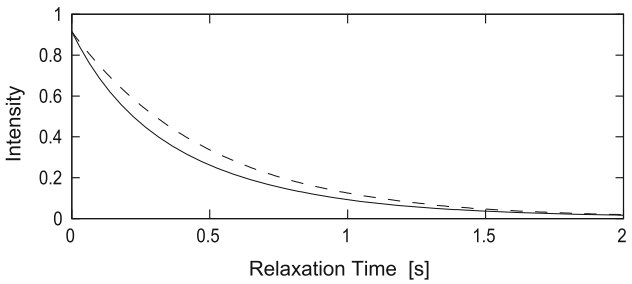


**Fig. 2** Longitudinal $^{15}$N relaxation curve (*solid line*) in the presence of H/D exchange and saturation transfer ($k = 5\ \mathrm{s}^{-1}$). For comparison the exponential decay in the absence of H/D exchange is shown (*dashed line*)

## Errors in the relaxation rates obtained from mono-exponential fits

Figure 3 displays apparent $^{15}$N relaxation rates for exchange-affected relaxation data, calculated using equations derived above, and least-squares fitted to mono-exponential decays.

Not surprisingly, the errors due to saturation transfer are most severe. The shape of the curves for the apparent

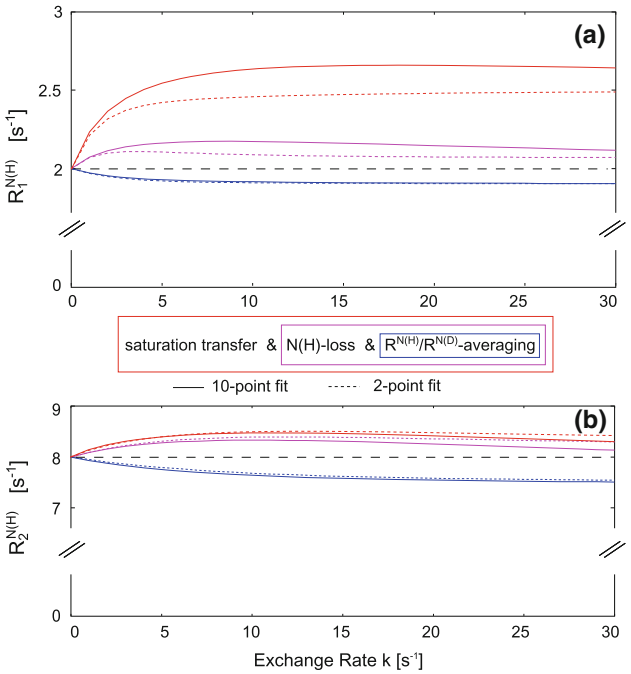


**Fig. 3** Apparent $R_1$ (**a**) and $R_2$ rates (**b**) as a function of the exchange rate $k$, calculated with (*red lines*) and without (*purple lines*) τ-dependent water saturation. Alternatively, curves for experiments just starting with equilibrium $^{15}$N magnetization are additionally shown (*blue lines*). The *solid lines* are obtained from least-squares fits of frequently sampled data ($R_1$-τ′s: 0.005, 0.01, 0.02, 0.04, 0.08, 0.16, 0.32, 0.64, 1.28, and 2.56 s; $R_2$-τ′s: 0.014, 0.028, 0.042, 0.056, 0.07, 0.098, 0.14, 0.21, 0.28 and 0.42 s) whereas the *dashed lines* are obtained by the two-point sampling strategy ($R_1$-τ′s: 0 and 0.65 s; $R_2$-τ's: 0 and 0.16 s). The *black dashed lines* describe the theoretical curves using rates of 2 $\mathrm{s}^{-1}$ ($R_1$) or 8 $\mathrm{s}^{-1}$ ($R_2$). 10 % deuterated solvent ($x = 0.1$) was assumed in all simulations, and the relaxation rates of deuterated species were assumed to be 1 $\mathrm{s}^{-1}$ ($R_1^{N(D)}$) or 2.9 $\mathrm{s}^{-1}$ ($R_2^{N(D)}$) respectively. The effect of water saturation was calculated using $p_{(\tau)} = 0.75e^{-1.7\tau}$ for the $R_1$- and $p_{(\tau)} = 0.7 + 0.24\tau - 2.7\tau^2$ for the $R_2$-experiment, respectively. (Color figure online)

relaxation rates in the absence of saturation transfer is influenced by the two counter-acting effects of $^{15}$N(H) magnetization loss due to H/D exchange (effect *ii*) and attenuated relaxation in the $^{15}$N(D) moieties (effect *iii*). With increasing exchange rates effect *ii* progressively influences the initial part of the relaxation curve while effect *iii* influences the entire curve similarly with the exception of the initial part. Depending on the sampling times, there will be an exchange rate by which effect *ii* affects the accuracy of the relaxation rates derived form mono-exponential fits to result in the largest deviations. Together with effect *iii* this determines the location of the maximum deviation from the true rates. For faster exchange the curve approximates an apparent relaxation rate that is $(1-x)R^{N(H)} + xR^{N(D)}$, corresponding to the limiting case for $k \rightarrow \infty$ of Eq. 4. The latter also corresponds to the value for very fast exchange when using the experiment modified to start with equilibrium $^{15}$N magnetization (blue curves).

Figure 3 clearly demonstrates that, regardless on the experimental scheme and independently of whether data are frequently sampled or not, considerable errors in apparent relaxation rates must be expected.

## Identifying exchange-affected relaxation data

In the favorable cases of data with very good S/N ratio and where the exchange rates are in a favorable range, one can identify such residues simply by visual inspection of the fitted curves. As shown in Fig. 4, a systematic error between the measured data and the fitted relaxation curves is then observed, and the data points for intermediate relaxation periods exceed the line from the fit. To which extent this behavior can be recognized, however, will strongly depend on which points are exactly sampled during the signal decay, and the quality of the experimental data.

Inconsistencies between the model function and the sampled data are detected by increased $\chi^2$ values. However, it is important to realize that in the case of a systematic deviation of the data from the model function the sum of squared residuals scales quadratic with signal intensity. Therefore $\chi^2$ values of weak cross-peaks are easily underestimated when a constant uncertainty in the peak-intensities is assumed. To correct for that, residue-specific uncertainties may be used which scale with the absolute cross-peak intensity (Skelton et al. 1993). Alternatively, time series data can be normalized, something that we consider easier to implement. Figure 5 compares $\chi^2$ values obtained from fits of normalized to those from non-normalized experimental data. The figure demonstrates that in the case of the non-normalized data the $\chi^2$ values for the exchanging residues 9 and 75, which have a four or three times lower signal intensity, are underestimated, while the $\chi^2$ values for the intense residues 16 and 26, that partially overlap, and for the most intense peak of residue 71 are overestimated.

## An alternative fitting scheme

In principle relaxation data obtained from experiments that preclude saturation transfer during the inter-scan delay (e.g. those with a water-purge element during the inter-scan delay) may be fitted according to Eq. 4. Unfortunately, no stable fits are obtained when all parameters ($R^{N(H)}$, $R^{N(D)}$, $k$, $x$ and $M_0$) are allowed to be varied. Therefore the following assumptions are introduced for $x$ and $R^{N(D)}$:

*For x:* On the basis of previous experimental work (Bowers and Klevit 1996; Khare et al. 1999; LiWang and Bax 1996; Englander and Poulsen, 1969) we assume fractionation factors close to 1.1 for solvent exposed NH's, and further postulate that fractionation factors should not exceed the range from 1.0 to 1.2.

*For $R^{N(D)}$*: Analytical expressions for the difference in relaxation rates of protonated and deuterated $^{15}$N nuclei (Xu et al. 2005; Vasos et al. 2006) are given in the Supplementary Material assuming that N–H and N–D bonds

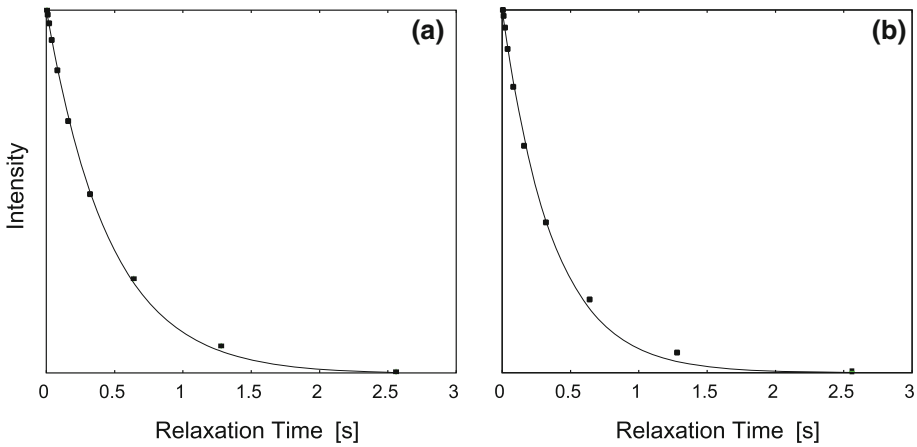


**Fig. 4** Mono-exponential fits of simulated $R_1$ decays. Peak intensities were calculated on the basis of Eq. 4 in (**a**) and when additionally taking effects from water saturation into account in (**b**). The parameters used for the simulations are: $R_1^{N(H)} = 2\ s^{-1}$, $R_1^{N(D)} = 1 s^{-1}$, $k = 5 s^{-1}$ and $x = 0.1$

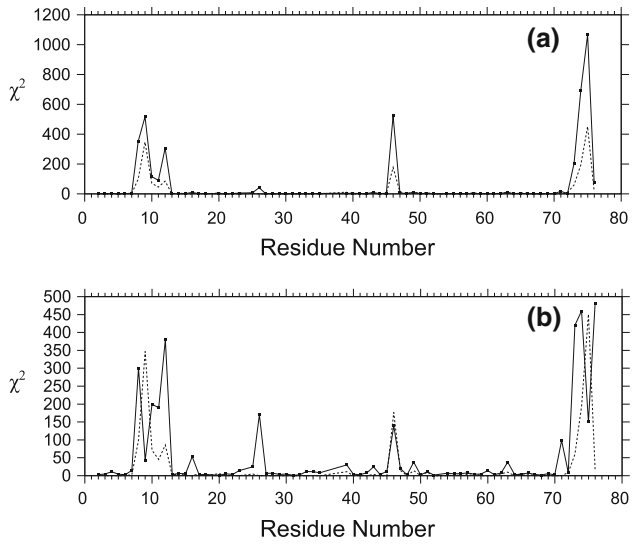


**Fig. 5** $\chi^2$ values obtained from mono-exponential fits of $R_1$ relaxation data of ubiquitin recorded with the wp-2-PT sequence (see below) when normalized (**a**) or non-normalized data (**b**) are fitted. Experimentally determined exchange rates are indicated by *dashed lines* at relative scale

are of same length (1.02 Å), a value of −172 ppm for the CSA, that the dynamics for N–H and N–D vectors are the same, that the molecule reorients isotropically, and that the dynamics and hence spectral densities are characterized according to the model-free approach (Lipari and Szabo 1982) in terms of an overall correlation time $\tau_m$, an effective correlation time $\tau_e$ and an order parameter $S^2$, the values of $\left(R^{N(H)} - R^{N(D)}\right)/R^{N(H)}$ obtained from a large number of calculations based on randomly varied values of $S^2$, $\tau_m$ and $\tau_e$ for different magnetic field strengths have been computed and are summarized in Table. 1. Based on these calculations we decided to replace $R^{N(D)}$ by $R^{N(H)}(1 - m)$ in the fitting function, with $m$ denoting the mean value calculated for a particular field strength.

Figure 6 displays the error (%) in the apparent relaxation rates when relaxation data calculated by Eq. 4 are least-square fitted to Eq. 4 with $x$ and $R^{N(D)}$ set to the above-described expected "mean-values" for 600 MHz data and 10 % $D_2O$. Further plots with different values of $x$ and $R_2$ along with the errors in $k$ can be found in the Supp. Mat. (Fig. S3,S4 and S5). The simulations indicate that the accuracy in the fitted relaxation rates obtained from multi-exponential fits are much improved for reasonable values of $x$ and $R^{N(D)}$. In addition, errors in single-exponential fits are smaller for larger values of $R_2$. In contrast, the accuracy in the exchange rates obtained from the multi-exponential fits strongly depend on the actual values of $x$ and $R^{N(D)}$, and errors of up to 15 % must be expected.

To probe the robustness of the fit of the relaxation and exchange rates when the data are affected by experimental

**Table 1** Mean and range for calculated values of $(R^{N(H)} - R^{N(D)})/R^{N(H)}$ using random values for $S^2$ (0.25–1), $\tau_m$ (2–10 ns) and $\tau_e$ (0.001–0.1 ns)

| Field strength (MHz) | Regarding $R_1$ | | Regarding $R_2$ | |
|---|---|---|---|---|
| | Mean ($m$) | Range | Mean ($m$) | Range |
| 500 | 0.55 | 0.45–0.65 | 0.7 | 0.65–0.75 |
| 600 | 0.5 | 0.4–0.6 | 0.64 | 0.58–0.7 |
| 700 | 0.45 | 0.35–0.55 | 0.59 | 0.52–0.64 |
| 800 | 0.4 | 0.3–0.5 | 0.53 | 0.46–0.6 |
| 900 | 0.35 | 0.28–0.46 | 0.48 | 0.42–0.54 |
| 1000 | 0.3 | 0.25–0.42 | 0.44 | 0.38–0.5 |

uncertainties (such as spectral noise) Monte-Carlo simulations were made. In these, synthetic relaxation data were generated and subsequently least-square fitted to Eq. 4 as described above or to a simple mono-exponential decay. In the course of the calculations we realized that the accuracy in the fitted $k$ is improved if $M_0$ is not allowed to vary but rather set to its value at $\tau = 0$. Accordingly, the volumes of the peaks were scaled such that the first data point at $\tau = 0$ was 1.0 for all residues.

Averages and confidence intervals of relaxation rates obtained from such simulations are shown in Fig. 7. Although in these calculations $R^{N(D)}$ and $x$ were both set to extremes in the expected range, the accuracy in the apparent relaxation rates significantly improves when using multi-exponential fits. We like to reiterate that the fit is much less robust with respect to exchange rates, even when noise levels are less than 0.5 % (Fig. S6 and S7). For that reason we recommend to interpret the exchange rates obtained from such fits only in a qualitative fashion.

## Experimental implementations

The standard experiment for measuring amide $^{15}N$ relaxation rates and two variants thereof are schematically depicted in Fig. 8. The modifications are motivated by the following considerations:

As the errors due to water saturation-transfer are most severe, care was taken to ensure that all experiments start with a constant amount of amide proton magnetization. A possibility to achieve this is to prevent water saturation during the relaxation period by applying band-selective $^1H$ decoupler pulses. This approach is widely used, but due to the severe radiation damping on cryogenic probes such an approach is difficult. Therefore it is technically easier to destroy any $^1H$ magnetization at the start of the inter-scan delay by applying a 90° $^1H$ pulse followed by a pulsed field gradient as shown in Fig. 8b, at the expense of a slight overall reduction of signal intensities for exchanging amide species.

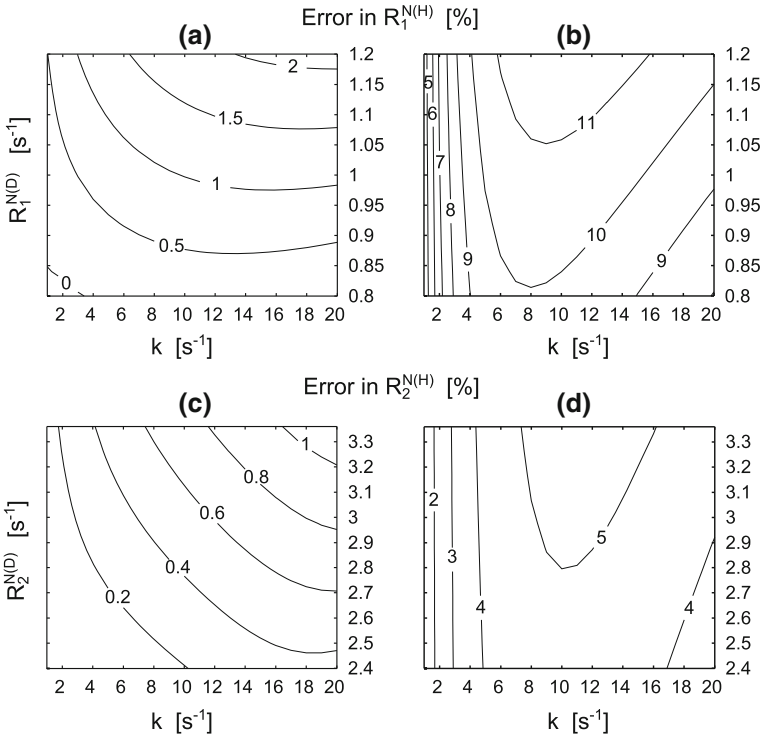


**Fig. 6** Relative error in $R_1$ (*top*) and $R_2$ (*bottom*) obtained from multi-exponential (*left*) or single-exponential (*right*) least-square fits as a function of $R_1^{N(D)}$ or $R_2^{N(D)}$ and $k$. The relaxation decays were calculated according to Eq. 4 with $R_1^{N(H)} = 2s^{-1}$ or $R_2^{N(H)} = 8\ s^{-1}$ and $x = 0.12$. For the $R_1$ data relaxation periods of 0.005, 0.01, 0.02, 0.04, 0.08, 0.16, 0.32, 0.64, 1.28 and 2.65 s and for the $R_2$ data values of 14, 28, 42, 56, 70, 98, 140, 210, 280 and 420 ms were used (600 MHz). The errors apply to the limiting case of noiseless data

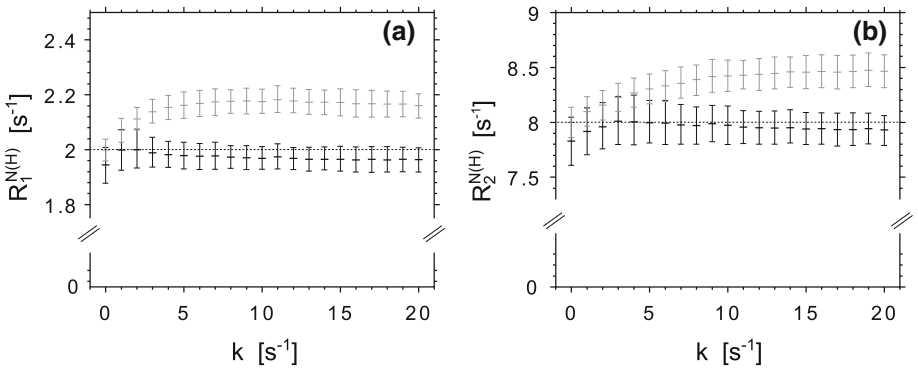


**Fig. 7** Mean values and confidence intervals (68 %) of fitted $R_1$ (**a**) and $R_2$ (**b**) as a function of the exchange rate obtained from 500 synthetic data sets generated on the basis of Eq. 4. Each data set was fitted to an multi-exponential (*black items*) or mono-exponential (*gray items*) decay. The *horizontal lines* indicate the theoretical $R_1$ (2 s$^{-1}$) and $R_2$ (8 s$^{-1}$) respectively. The relaxation delays were chosen the same as in Fig. 6, $R_1^{N(D)} = 0.8s^{-1}$, $R_2^{N(D)} = 2.4\ s^{-1}$ and $x = 0.1$. An random error of ±1 % of the maximal signal amplitude at $\tau = 0$ was added to each data point. For additional plots see the Fig. S6 and S7

Additionally, we have recognized that the quality of the relaxation data improves when the water magnetization is purged for a second time during the zz-period during the initial refocused INEPT (by gradient g2). This will eliminate the water magnetization which otherwise creates a τ-dependent radiation damping field that might interact with amide magnetization during the back-INEPT and thereby results in further modulation in signal intensity. While such subtle errors may be negligible when using mono-exponential fits, they can no longer be ignored when using multi-exponential fits.

Figure 8c depicts the variant that simply starts with $^{15}$N magnetization. In this sequence a water purge element is employed to ensure that $^{15}$N magnetization is equally affected by $^{1}$H–$^{15}$N cross-relaxation, independent of the degree by which water was saturated during the relaxation period τ.

## Experimental section

### NMR spectroscopy

All data were recorded using a sample of 1 mM $^{13}$C, $^{15}$N-labeled human ubiquitin in 90 % $H_2O$/10 %$D_2O$ at pH 7, 50 mM NaPI, 0.02 % $NaN_3$.

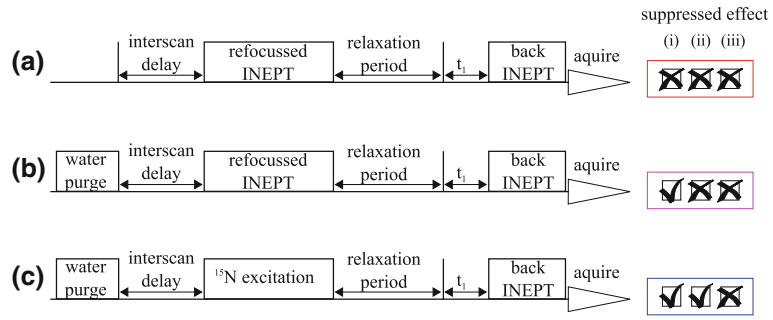


**Fig. 8** Schematic representation of **a** the standard double polarization-transfer (2-PT)-, **b** the "water purged"- 2-PT (wp-2-PT) and **c** the single PT (1-PT) experiments for measuring amide $^{15}$N relaxation rates. *Boxes* on the *right* indicate, which effects are suppressed. The same coloring scheme as in Fig. 3 is used. For details of the experiments see Figure S8

All NMR experiments were performed at 296 K on a Bruker AV-600 spectrometer equipped with a *z*-gradient TCI cryoprobe. Pulse sequences used for measuring relaxation rates basically correspond to those reported by Farrow et al. (1994) with the modifications described above with more details provided in the Supp. Mat. (Fig. S8). The MEXICO experiment (Gemmecker et al. 1993) was modified to use a HSQC instead of an HMQC scheme (see Fig. S9). In all sequences special attention was paid to the proper manipulation of water magnetization in the presence of strong radiation damping. In all experiments the $^{1}$H carrier was set to the water signal (4.7 ppm), the $^{15}$N carrier to 117.5 ppm, and the $^{13}$C carrier for the adiabatic pulse to 119.5 ppm.

Seven MEXICO experiments with different exchange delays $T_{EX}$ and a reference spectrum were collected in randomized order. The exchange delays were set to 5, 10, 20, 50, 100, 200 and 400 ms. For each experiment 1,024 × 128 ($^{1}$H × $^{15}$N) complex points have been collected with 8 scans per $t_1$ increment and an inter-scan delay of 4 s. In case of $R_1$ 10 experiments for each of the three experimental schemes with relaxation delays τ of τ = 0, 10, 20, 40, 80, 160, 320, 640, 1280 and 2000 ms were measured in randomized order. 1,024 × 100 ($^{1}$H × $^{15}$N) complex points were recorded with 8 scans per $t_1$ increment and an inter-scan delay of 2 s.

Similarly for $R_2$, 10 experiments with delay settings of τ = 0, 17, 34, 51, 68, 102, 136, 187, 254 and 390 ms were recorded for all 3 schemes, with 1,024 × 100 ($^{1}$H × $^{15}$N) complex points, 8 scans per $t_1$ increment and an inter-scan delay of 1.8 s.

All data were processed using the software TOPSPIN 2.1. Time domain data in the $^{15}$N dimension were doubled by linear prediction, and a squared cosine window function was applied in both dimensions. Zero filling was used in both dimensions to yield spectra of 2, 048 × 1, 028 ($^{1}$H × $^{15}$N) size.

## Data analysis

Peak volumes of all spectra were extracted using the software SPSCAN (Glaser and Wüthrich 1997). Non-linear least squares fits were obtained using the Levenberg-Marquad algorithm using home-written routines.

In the analysis of amide exchange peak volumes were normalized to the reference spectrum and the exchange rates $k$ were then obtained by two-parameter ($k$ and $R_H$) least-squares fits to the equation (Schwartz and Cutnell 1983; Mori et al. 1996)

$$I_{(T_{EX})} = C\frac{k}{k - R_w + R_H}\left(\mathrm{e}^{-R_w T_{EX}} - \mathrm{e}^{-(k+R_H)T_{EX}}\right) \tag{9}$$

where $R_w$ and $R_H$ are the longitudinal relaxation rates of water and amide protons respectively, and $C$ is a factor describing to what extent the thermal equilibrium water magnetization ($M_{eq}$) becomes attenuated to result in a steady-state magnetization ($M_{st}$) prior to the exchange time $T_{EX}$, thus $C = M_{st}/M_{eq}$. This factor was determined in separate experiments to be 0.95. The longitudinal relaxation rate of water was measured to be 0.32s$^{-1}$ with an inversion-recovery experiment using a weak gradient during the recovery delay to prevent radiation damping.

Excellent fits were obtained for residues for which magnetization is recovered to an extent >5 % in the MEXICO sequence, and this criterion was used to identify exchanging residues.

Relaxation rates were obtained by either least-squares fits of normalized time series data to simple mono-exponential decays of the form $I(t) = I_0 \exp(-Rt)$ or to the multi-exponential function

$$I(t) = \left[\cosh(\frac{g}{2}t) - \frac{1}{g}(k(2x-1) + \Delta R)\sinh(\frac{g}{2}t)\right] \times \mathrm{e}^{-\frac{R(2-m)+k}{2}t} \tag{10}$$

with

$$g = \sqrt{\Delta R^2 + 2k(2x-1)\Delta R + k^2}$$

and

$$\Delta R = mR$$

Therein $x$ was set to 0.11 and the values of $m$ according to Tab. 1 to 0.5 for $R_1$ data and to 0.64 for $R_2$ data.

## Results

To verify the theoretical considerations described above experimental data were recorded using a sample of human ubiquitin at $pH \sim 7$. $R_1$ and $R_2$ rates were measured using the sequences depicted in Fig. 8 and described in more detail in the Supp. Mat. Moreover, the amide proton exchange rates were measured using the MEXICO experiment (Gemmecker et al. 1993). 69 out of the total 73 non-proline cross peaks from the HSQC-type spectra were sufficiently resolved and analyzed. The assignment was based on the chemical shifts reported by Wickliffe et al. (2011) (BMRB entry 17439).

### Exchange rates

Figure 9 displays the exchange rates obtained from the MEXICO experiment. Arrows indicate residues for which the magnetization build-up curves reaches at least 5 % of the values obtained when the isotope filter is omitted. For all these residues the data are fitted well and the simultaneously derived $R_1$ rates are in the reasonable range of a few Hertz. The exchange rates follow a similar pattern but are roughly two times larger than those reported by Brand et al. (2007) and Fan et al. (2011) for ubiquitin samples at pH 5.8 and 24 °C or for pH 6.8 and 25 °C, respectively. Considering the strong dependence of the amide exchange rate on the pH this difference can be easily attributed to the different pH of 7.0 used in our study.

### $R_1$ relaxation

The $R_1$ rates obtained from mono-exponential fits of relaxation data measured by all three experimental schemes of Fig. 8 are depicted in Fig. 10a. The variation in relaxation rates for residues with pronounced amide proton exchange (see Fig. 9), that display increased values of $\chi^2$ in the mono-exponential fits (see Fig. 5) is clearly seen. In contrast, for regions with reduced solvent exchange such as those from helix H1 relaxation rates obtained from the three experiments are very similar. Interestingly, the $R_1$ rates obtained from the standard sequence (Fig. 8a) are slightly increased throughout almost the whole peptide. This may be due to either a small exchange contribution of less than 1 $s^{-1}$ (compare Fig. 3) or more likely due to NOE effects.

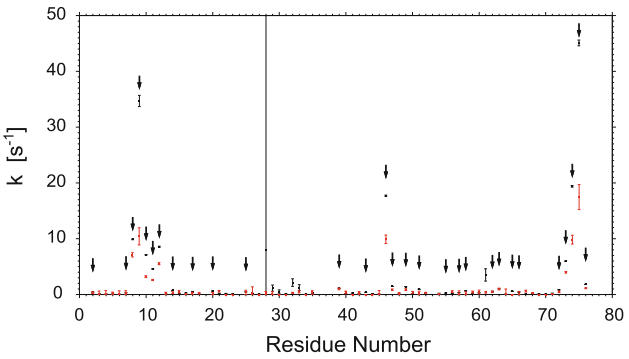


**Fig. 9** Amide proton exchange rates of ubiquitin as determined by the MEXICO experiment (*black*). The *error-bars* indicate asymptotic standard errors. Residues with reliable exchange rates are indicated by *arrows*. Amide proton exchange rates obtained from multi-exponential fits of relaxation data using the sequence wp-2-PT are shown in *red* (Fig. 8b). (Color figure online)

The relative difference in $R_1$ rates when using mono- or multi-exponential fits is displayed in Fig. 11 revealing differences as large as 10 %. For further plots of residuals see Supp. Mat. Fig. S10. These clearly demonstrate the improvements in the multi-exponential fits.

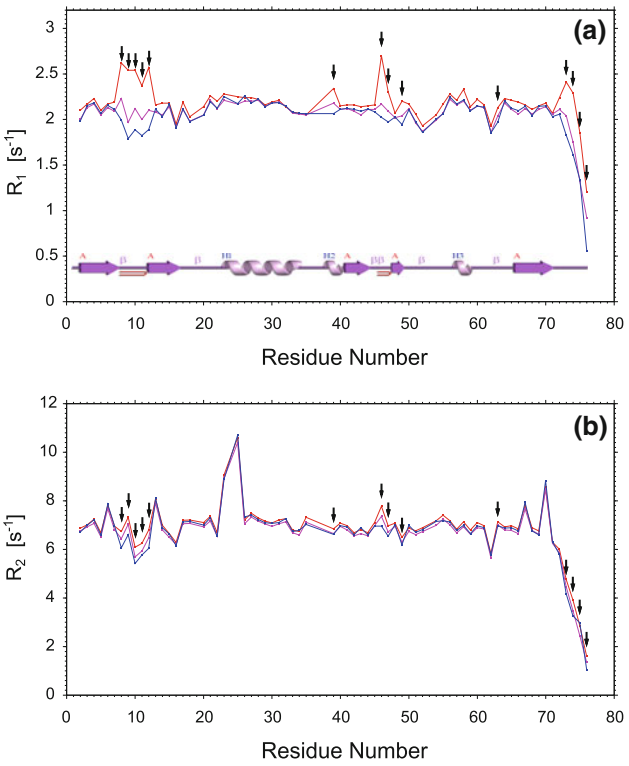


**Fig. 10** **a** $R_1$ and **b** $R_2$ $^{15}$N relaxation rates using the sequences from Fig. 8a (*red*), 8b (*purple*) and 8c (*blue*). The *arrows* indicates residues with exchange rates >1 $s^{-1}$ as measured in the MEXICO experiment. For comparison the location of secondary structure is also depicted. (Color figure online)

### $R_2$ relaxation

In the case of $R_2$ measurements the effects of amide exchange are much less severe and deviations from mono-exponential decays seem to be dominated by $^{15}$N offset effects during the CPMG sequence. The variation in $R_2$ rates recorded by the three different experimental schemes are shown in Fig. 10b. For amide species with pronounced H/D exchange (indicated by arrows) the $R_2$ rates follows the expected trend $R_2$(2-PT sequence) $>$ $R_2$(wp-2-PT sequence) $>$ $R_2$(1-PT sequence), while the rates for non-exchanging moieties are very similar, again with a slight increase of $R_2$ values recorded with the 2-PT sequence.

Interestingly, we noticed that the variation of $\chi^2$ values obtained by mono-exponential fits is much larger than for $R_1$ rates, and largely a function of the $^{15}$N offset. This is depicted in Fig.12 and indicates systematic errors introduced by the CPMG sequence. Hence we recommend to refrain from applying multi-exponential fits to $R_2$ data. When still using multi-exponential fits enhanced $k$ rates were obtained for those with fast proton exchange but also for those three residues with a large $^{15}$N offset (see Fig. S12).

Figure 13 compares the $R_1$ and $R_2$ relaxation rates for data using the wp-2-PT sequence and obtained from mono- or multi-exponential fits with those reported by Tjandra et al. (1995) for a sample of U-$^{15}$N ubiquitin at 27 °C and pH 4.7. In the case of our data rates from multi-exponential fits are used for all residues with $\chi^2 > 50$ according to Fig. 5a, while data derived from mono-exponential fits were used otherwise. These $R_1$ and $R_2$ relaxation rates have a similar trend as those reported by Tjandra et al. (1995) with a slight decrease ($0.05 \pm 0.04 s^{-1}$) for $R_1$ and an increase ($1.0 \pm 0.4 s^{-1}$) for $R_2$, due to a difference in temperature (4 °C lower in our measurements), and possibly due to additional relaxation contributions from $^{13}$C nuclei and slight differences in pH and concentration of the protein.

We also investigated to which extent an alternative two-point sampling strategy affects errors. A comparison of the relaxation rates as obtained from the two-point and the multi-point sampling scheme can be found in the Supp. Mat. Fig. S13. The variation in the extracted rate constants

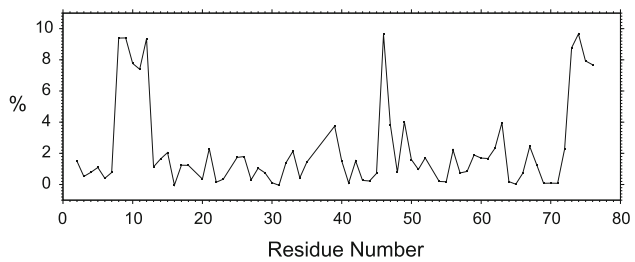


**Fig. 11** Percentage difference between $R_1$ rates obtained from mono- and multi-exponential fits

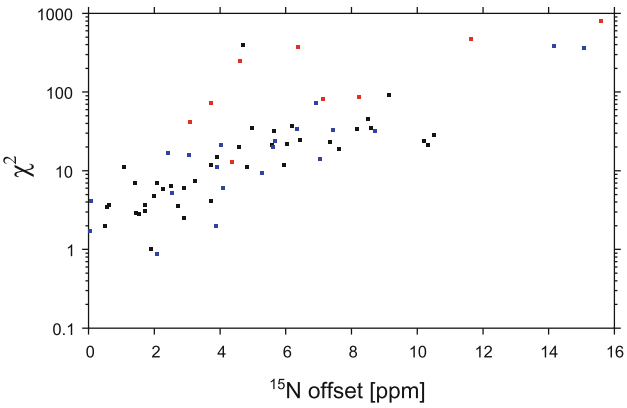


**Fig. 12** $\chi^2$ values (at logarithmic scale) obtained from mono-exponential fits of relaxation data measured with the wp-2-PT sequence as a function of the $^{15}$N offset. *Black dots* represent residues with no exchange, *blue dots* those with exchange rates $k < 2 s^{-1}$ and *red dots* those with exchange rates $k > 2 s^{-1}$ as determined by the MEXICO experiment. (Color figure online)

is in agreement with the simulations (Fig. 3), in that for residues with elevated hydrogen exchange and when using the 2-PT- and wp-2-PT-sequences, the two-point fitted $R_1$ rates are smaller than those derived from multi-point fits. Less significant differences in the derived rate constants are observed for the $R_2$ data.

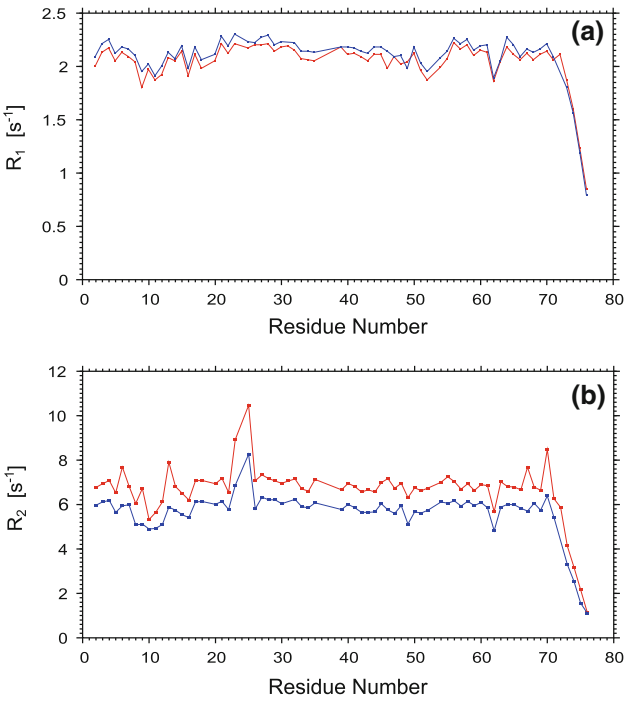


**Fig. 13** Comparison of $R_1$ (**a**) or $R_2$ (**b**) rates obtained from mono- or multi-exponential fits from data obtained with the wp-2-PT sequence (*red*) with those reported by Tjandra et al. (1995) (*blue*). For all residues with $\chi^2 > 50$ (compare 5a) values from the multi-exponential fits were used. (Color figure online)

Furthermore, we have compared $R_1$ and $R_2$ rates derived from peak heights instead of peak volumes. However, differences in the rate constants are usually within the standard error of the fits.

## Discussion

The interplay of function and dynamics of biomolecules has increasingly attracted interest over the last decade. Backbone dynamics are mostly evaluated from $^{15}$N relaxation. Particularly, when more subtle details of dynamics such as rates of interconversion processes and internal correlation times are computed it is of prime importance that the underlying relaxation rates are determined to high precision. Herein, we have systematically investigated the effects of amide exchange on $^{15}$N longitudinal and transverse relaxation rates as a potential source of error. These may for example be present when studying partially unfolded proteins at elevated values of the pH. Since dynamics may be of particular interest in these systems methods to remove the detrimental effects of solvent exchange on relaxation data are required.

The contributions to these relaxation processes may result in subtle changes of the decay curves that may not be immediately recognized. We discovered that errors up to 10 % may be present in the $R_1$ rates for rapidly exchanging residues. We could demonstrate that in the presence of fast exchange reasonably precise values can still be extracted when using pulse-experiments designed to remove the effects from saturation transfer during the inter-scan delay and when the exchange-affected experimental $R_1$ data points are fitted to multi-exponential decays. Moreover, effects in samples containing lower contents of $D_2O$ are expected to be lower. Although it may be tempting to fit all data to a multi-exponential model we suggest to refrain from doing so because for exchange rates close to zero a slight underestimation of the relaxation rates may result, and multi-exponential fits additionally induce the risk for over-fitting relaxation data. Therefore we recommend to use multi-exponential fits only for (1) residues for which elevated amide exchange rates ($k \geq 1s^1$) have been determined experimentally or (2) for residues which are poorly fitted by the mono-exponential model as indicated by increased $\chi^2$ values and increased residuals of the fit.

The errors in the exchange rates obtained from multi-exponential fits (Fig. 9) are much higher than expected from Supplementary Figure 3 and 6, considering the low uncertainty in the $R_1$ data ($< 0.5$ %). Interestingly the accuracy improves when the parameter $x$ is not restricted to a value of 0.11 but also fitted simultaneously. For the fast exchanging residues (8–12, 46, 73–75) we obtain values of $x$ between 0.067 and 0.1, and the low value of 0.067 is found for Thr9, a residue for which an exceptional low fractionation factor was reported by Bowers and Klevit (2000).

It is interesting to compare our results to the findings of a recent paper of Chen and Tjandra (2011). The authors observed that the $R_1$ values are underestimated when water magnetization is purged in the center of the refocused INEPT-element compared to when using a sequence designed for minimal water saturation. In both sequences care is taken to prevent water saturation in the course of $^1$H decoupling during the relaxation period. As they noted, in such a case the purged water magnetization gradually recovers during the relaxation decay, such that saturation transfer is less severe for longer τ's resulting in a decrease of the determined relaxation rates.

## References


Abragam A (1961) The principles of nuclear magnetism: the international series of monographs on physics. Clarendon Press, Oxford

Bowers P, Klevit R (2000) Hydrogen bond geometry and $^2$H/$^1$H fractionation in proteins. J Am Chem Soc 122(6):1030–1033

Bowers PM, Klevit RE (1996) Hydrogen bonding and equilibrium isotope enrichment in histidine-containing proteins. Nat Struct Biol 3:522–531

Boyd J, Hommel U, Campbell I (1990) Influence of cross-correlation between dipolar and anisotropic chemical shift relaxation mechanisms upon longitudinal relaxation rates of $^{15}$N in macromolecules. Chem Phys Lett 175:477–482

Brand T, Cabrita EJ, Morris GA, Günther R, Hofmann HJ, Berger S (2007) Residue-specific NH exchange rates studied by NMR diffusion experiments. J Magn Reson 187:97–104

Carver J, Richards R (1972) A general two-site solution for the chemical exchange produced dependence of $T_2$ upon the Carr-Purcell pulse separation. J Magn Reson 6:89–105

Cavanagh J, Fairbrother WJ, Palmer III AG, Skelton NJ, Rance M (1996) Protein NMR spectroscopy: principles and practice. Academic Press, London

Chen K, Tjandra N (2011) Water proton spin saturation affects measured protein backbone $^{15}$N spin relaxation rates. J Magn Reson 213:151 – 157

Chevelkov V, Diehl A, Reif B (2008) Measurement of $^{15}$ N-$T_1$ relaxation rates in a perdeuterated protein by magic angle spinning solid-state nuclear magnetic resonance spectroscopy. J Chem Phys 128:052,316

Chevelkov V, Xue Y, Rao DK, Forman-Kay JD, Skrynnikov NR (2010) $^{15}$N$^{H/D}$-SOLEXSY experiment for accurate measurement of amide solvent exchange rates: application to denatured drkN SH3. J Biomol NMR 46:227–244

Dayie K, Wagner G, Lefèvre J (1996) Theory and practice of nuclear spin relaxation in proteins. Annu Rev Phys Chem 47:243–282

del Amo JML, Fink U, Reif B (2010) Quantification of protein backbone hydrogen-deuterium exchange rates by solid state NMR spectroscopy. J Biomol NMR 48:203–212

Dellwo MJ, Wand AJ (1991) Systematic bias in the model-free analysis of heteronuclear relaxation. J Magn Reson 91:505–516

Englander S, Poulsen A (1969) Hydrogen-tritium exchange of the random chain polypeptide. Biopolymers 7:379–393

Fan JS, Lim J, Yu B, Yang D (2011) Measurement of amide hydrogen exchange rates with the use of radiation damping. J Biomol NMR 51:151–162

Farrow NA, Muhandiram R, Singer AU, Pascal SM, Kay CM, Gish G, Shoelson SE, Pawson T, Forman-Kay JD, Kay LE (1994) Backbone dynamics of a free and phosphopeptide-complexed Src homology 2 domain studied by $^{15}$N NMR relaxation. Biochemistry 33:5984–6003

Farrow NA, Zhang O, Forman-Kay JD, Kay LE (1995) Comparison of the backbone dynamics of a folded and an unfolded SH3 domain existing in equilibrium in aqueous buffer. Biochemistry 34:868–878

Fischer M, Majumdar A, Zuiderweg E (1998) Protein NMR relaxation: theory, applications and outlook. Prog Nucl Magn Reson Spectrosc 33:207–272

Gemmecker G, Jahnke W, Kessler H (1993) Measurement of fast proton exchange rates in isotopically labeled compounds. J Am Chem Soc 115:11,620–11,621

Glaser RW, Wüthrich K (1997) SPSCAN. http://gaudi.molebio.uni-jena.de/rwg/spscan

Grzesiek S, Bax A (1993) The importance of not saturating water in protein NMR. Application to sensitivity enhancement and NOE measurements. J Am Chem Soc 115:12,593–12,594

Idiyatullin D, Daragan VA, Mayo KH (2001) Improved measurement of $^{15}N-\{^{1}H\}$ NOEs in the presence of H(N)-water proton chemical exchange. J Magn Reson 153:138–143

Jin D, Andrec M, Montelione G, Levy R (1998) Propagation of experimental uncertainties using the Lipari-Szabo model-free analysis of protein dynamics. J Biomol NMR 12:471–492

Jones J, Hodgkinson P, Barker A, Hore P (1996) Optimal sampling strategies for the measurement of spin-spin relaxation times. J Magn Reson 113:25–34

Kay L, Nicholson L, Delaglio F, Bax A, Torchia D (1992) Pulse sequences for removal of the effects of cross correlation between dipolar and chemical-shift anisotropy relaxation mechanisms on the measurement of heteronuclear $T_1$ and $T_2$ values in proteins. J Magn Reson 97:359–375

Khare D, Alexander P, Orban J (1999) Hydrogen bonding and equilibrium protium-deuterium fractionation factors in the immunoglobulin G binding domain of protein G. Biochemistry 38:3918–3925

Korzhnev D, Billeter M, Arseniev AS, Orekhov V (2001) NMR studies of Brownian tumbling and internal motions in proteins. Prog Nucl Magn Reson Spectrosc 38:197

Korzhnev DM, Tischenko EV, Arseniev AS (2000) Off-resonance effects in $^{15}$N $T_2$ CPMG measurements. J Biomol NMR 17: 231–237

Li Y, Montelione G (1994) Overcoming solvent saturation-transfer artifacts in protein NMR at neutral pH. Application of pulsed field gradients in measurements of $^{1}H-{}^{15}N$ Overhauser effects. J Magn Reson 105:45–51

Li Y Y, Montelione G (1993) Solvent saturation-transfer effects in pulsed-field-gradient heteronuclear single-quantum-coherence (PFG-HSQC) spectra of polypeptides and proteins. J Magn Reson 101:315–319

Lipari G, Szabo A (1982) Model-free approach to the interpretation of nuclear magnetic resonance relaxation in macromolecules. 1. Theory and range of validity. J Am Chem Soc 104:4546–4559

LiWang A, Bax A (1996) Equilibrium protium/deuterium fractionation of backbone amides in $U-{}^{13}C/{}^{15}N$ labeled human ubiquitin by triple resonance NMR. J Am Chem Soc 118: 12,864–12,865

Liwang AC, Bax A (1997) Solution NMR characterization of hydrogen bonds in a protein by indirect measurement of deuterium quadrupole couplings. J Magn Reson 127:54–64

Mori S, Abeygunawardana C, van Zijl PC, Berg JM (1996) Water exchange filter with improved sensitivity (WEX II) to study solvent-exchangeable protons. Application to the consensus zinc finger peptide CP-1. J Magn Reson 110:96

Morin S (2011) A practical guide to protein dynamics from $^{15}$ N spin relaxation in solution. Prog Nucl Magn Reson Spectrosc 59: 245–262

Myint W, Gong Q, Ishima R (2009) Practical aspects of $^{15}$ N CPMG transverse relaxation experiments for proteins in solution. Concepts Magn Reson 34:63–75

Orekhov V, Korzhnev D, Diercks T, Kessler H, Arseniev AS (1999) $^{1}H-{}^{15}N$ NMR dynamic study of an isolated α-helical peptide (1–36)-bacteriorhodopsin reveals the equilibrium helix-coil transitions. J Biomol NMR 14:345–356

Palmer A, Cavanagh J, Wright P, Rance M et al (1991) Sensitivity improvement in proton-detected two-dimensional heteronuclear correlation NMR spectroscopy. J Magn Reson 93:151–170

Palmer III A, Skelton N, Chazin W, Wright P, Rance M (1992) Suppression of the effects of cross-correlation between dipolar and anisotropic chemical shift relaxation mechanisms in the measurement of spin-spin relaxation rates. Mol Phys 75:699–711

Ross A, Czisch M, King G (1997) Systematic errors associated with the CPMG pulse sequence and their effect on motional analysis of biomolecules. J Magn Reson 124:355–365

Schwartz A, Cutnell J (1983) One-and two-dimensional NMR studies of exchanging amide protons in glutathione. J Magn Reson 53: 398–411

Skelton N, Palmer A, Akke M, Kordel J, Rance M, Chazin W (1993) Practical aspects of two-dimensional proton-detected $^{15}$ N spin relaxation measurements. J Magn Reson 102:253−264

Tjandra N, Feller S, Pastor R, Bax A (1995) Rotational diffusion anisotropy of human ubiquitin from $^{15}$N NMR relaxation. J Am Chem Soc 117:12,562–12,566

Vasos PR, Hall JB, Kümmerle R, Fushman D (2006) Measurement of $^{15}$N relaxation in deuterated amide groups in proteins using direct nitrogen detection. J Biomol NMR 36:27–36

Wickliffe K, Lorenz S, Wemmer D, Kuriyan J, Rape M (2011) The mechanism of linkage-specific ubiquitin chain elongation by a single-subunit E2. Cell 144:769–781

Xu J, Millet O, Kay LE, Skrynnikov NR (2005) A new spin probe of protein dynamics: nitrogen relaxation in $^{15}$N–$^{2}$ H amide groups. J Am Chem Soc 127:3220–3229

Yip G, Zuiderweg E (2004) A phase cycle scheme that significantly suppresses offset-dependent artifacts in the $R_2$-CPMG $^{15}$ N relaxation experiment. J Magn Reson 171:25–36

Yip G, Zuiderweg E (2005) Improvement of duty-cycle heating compensation in NMR spin relaxation experiments. J Magn Reson 176:171–178